



ORIGINAL ARTICLE

Green synthesis of chitosan-stabilized silver-colloidal nanoparticles immobilized on white-silica-gel beads and the antibacterial activities in a simulated-air-filter



Muhammad Iqbal Hidayat^a, Muhammad Adlim^{a,b,*}, Ilham Maulana^c,
Suhartono Suhartono^d, Zinatul Hayati^e, Noor Hana Hanif Abu Bakar^f

^a Graduate School of Mathematics and Applied Science, Universitas Syiah Kuala, Darussalam Banda Aceh 23111, Indonesia

^b Chemistry Department, FKIP, Universitas Syiah Kuala, Darussalam Banda Aceh 23111, Indonesia

^c Chemistry Department, Faculty of Mathematics and Natural Sciences, Universitas Syiah Kuala, Darussalam Banda Aceh 23111, Indonesia

^d Biology Department, Faculty of Mathematics and Natural Sciences, Universitas Syiah Kuala, Darussalam Banda Aceh 23111, Indonesia

^e Department of Microbiology, School of Medicine, Universitas Syiah Kuala, Banda Aceh, Indonesia

^f School of Chemical Sciences, Universiti Sains Malaysia, 11800 USM, Penang, Malaysia

Received 18 September 2021; accepted 24 November 2021

Available online 27 November 2021

KEYWORDS

Immobilization;
Silver nanoparticles;
Chitosan;
Antibacterial;
Air filter

Abstract This study explored the green synthesis and immobilization of colloidal silver nanoparticles (AgNPs) on a solid compatible support. Its antibacterial properties in reusable air filters are also discussed. The chitosan stabilized colloidal AgNPs (chi-AgNPs) were prepared using visible light irradiation in methanol. The UV-Vis, FTIR spectra, and TEM confirmed the chi-AgNPs formation. The immobilization technique of chi-AgNPs on the surface of white-silica-gel beads, which was previously coated chitosan (chi-SiG), was effective. The immobilized silver particles (AgNPs-[chi-SiG]) were solid, stable, dispersed, and nano-size. Both AgNPs-[chi-SiG] and chi-SiG exhibited antibacterial properties and prevented the growth of Gram-positive (*Staphylococcus aureus*) and

* Corresponding author at: Graduate School of Mathematics and Applied Science, Universitas Syiah Kuala, Darussalam Banda Aceh 23111, Indonesia.

E-mail address: adlim@unsyiah.ac.id (M. Adlim).

Peer review under responsibility of King Saud University.



Production and hosting by Elsevier

Gram-negative (*Escherichia coli*) bacteria in agar media. Air filter containing the AgNPs-[chi-SiG] showed high antibacterial activity against *Bacillus subtilis* in the air.

© 2021 The Authors. Published by Elsevier B.V. on behalf of King Saud University. This is an open access article under the CC BY-NC-ND license (<http://creativecommons.org/licenses/by-nc-nd/4.0/>).

1. Introduction

There has been an increasing emphasis on developing green synthesis to reduce harmful solvents and toxic reagents in the past few decades. The use of environmentally friendly solvents and multipurpose reagents that serve as the reducing agent are significant issues in green nanoparticle production. The nanoparticles are usually prepared either by physical (Zhang et al., 2016; Kang et al., 2019) or chemical methods (Gakiya-Teruya et al., 2019; Targhi et al., 2021). In chemical processes, many procedures involve stabilizers and reducing agents that are toxic and harmful to the environment (Shanmuganathan et al., 2019). Research has shown that the biological method is a rapid single-step method, cost-effective and eco-friendly, and without toxic chemicals (Velusamy et al., 2016; Gonca et al., 2021; Hashemi et al., 2021). The biological methods usually employ plant extracts as the reducing agents or the stabilizers for AgNPs. Biological materials, including plant extracts, easily decompose and might not be long-lasting (Zhang et al., 2018; Alsammaraie et al., 2018; Senthilkumar et al., 2019). A simple procedure to minimize the chemical toxicity of stable and preservable nanoparticles is demand for metallic nanoparticle synthesis. Several simple studies have been introduced involving chitosan (natural polymer from crustacean shells) as stabilizers and reducing agents for colloidal gold nanoparticles (Adlim & Bakar, 2008). Chitosan stabilized colloidal silver nanoparticles (chi-AgNPs) prepared with visible photo-irradiation is an alternative for green chi-AgNPs synthesis to prepare relatively dispersed nanoparticles and narrower size distribution (Adlim, 2006a). Chitosan has characteristics as biodegradable polymer, film-forming ability, antimicrobial activities, biodegradability, and non-toxicity. It is widely used in numerous applications (Sundaram et al., 2016; Divakar et al., 2017; Ranjani et al., 2019; Ye et al., 2019; Awais et al., 2021; Valencia et al., 2021). Chitosan has amino groups that serve as lone pair electrons to attract Ag^+ ions for coordination bond formation (Wang et al., 2015).

Among the antimicrobial nanoparticles, AgNPs has gained significant attention due to their antimicrobial activity against a wide range of microorganism (Wang et al., 2017). AgNPs can kill more than 650 types of pathogenic microbes, such as bacteria (Senthilkumar et al., 2017; Angulo-Pineda et al., 2019; Kanniah et al., 2021), fungi (Zhang et al., 2019; Dutta et al., 2020) and viruses (Hamouda et al., 2021; García-Serradilla & Risco, 2021). AgNPs exhibit antimicrobial efficacy due to their large surface area, thermal stability, and Ag^+ release rate, depending on the silver type, size, and shape. Compared to bulk metal or salts, AgNPs achieve the slow and controlled Ag^+ release, contributing to their antimicrobial endurance (Mokhena & Luyt, 2017; Raman et al., 2017). Most of the bioactivity testings were focused on colloidal AgNPs, which has some constraints in scaling-up and broader application. The colloidal system is less efficient, not easily separated from the liquid substrate, and less compatible for continuous use and regeneration (Alamgholiloo et al., 2020; Wijesena et al., 2020).

In the present research, we studied the immobilization of colloidal AgNPs on white-silica-gel beads that are a compatible size for the gas antibacterial filter. The immobilization technique of AgNP on silica beads has not been much known. An immobilization model was introduced on bimetallic Pd/Au on titania powder (Adlim & Bakar, 2013). The immobilization challenges are how to keep metal nanoparticles stable in proper particle size in solid-state form, but the particle size and distribution are comparable to the colloidal phase. The stabilizer

and an adhesive are required to adhere colloidal nanoparticles onto the support. Still, the nanoparticles remain dispersed, and the stabilizer shall not cover up the nanoparticle surface.

Some researchers have used AgNPs for air filtration purposes due to their antibacterial properties. The AgNPs directly adhered onto the High-Efficiency Particulate Air (HEPA) filter cloth. This may reduce the air-fluent rate and is not easily regenerated (Venkatesan et al., 2017; Ju et al., 2021; Ji et al., 2021). Thereby, chi-AgNPs immobilized on the white-silica gel are studied as the alternative solution to address this issue. The antimicrobial activity is represented by Gram-negative and Gram-positive bacteria in a simulated air filter.

2. Materials and method

2.1. Materials and equipment

Medium molecular weight chitosan (~400,000) purchased from Sigma-Aldrich (Indonesia) and white-silica-gel beads (sorbed India production; spherical, $\varnothing \sim 3$ cm with specification refer to <https://www.silicagel-desiccant.com/silica-gel-white>) were purchased from the local market (Indonesia). Acetic acid glacial (CH_3COOH) solution (99.8%), silver nitrate (AgNO_3) crystal, and methanol (CH_3OH) were of analytical grade and purchased from Merck KGaA (Indonesia). Distilled water (H_2O) was purchased from the Chemistry Laboratory of Syiah Kuala University (Indonesia). *Escherichia coli* (*E. coli*, ATCC 25922), *Staphylococcus aureus* (*S. aureus*, ATCC 25923), *Bacillus subtilis* (*B. subtilis*, ATCC 6633), Mueller-Hinton Agar (MHA), and Nutrient Agar (NA) were all obtained from Dipa Puspa Labsains (Indonesia). All chemicals were used without further purification.

2.2. Preparation and characterization of colloidal chi-AgNPs

Colloidal chi-AgNPs were prepared following a previous study (Adlim, 2006a) with some modifications. It was prepared by dissolving 0.600 g of chitosan in 100 mL of 1.5% (v/v) aqueous acetic acid under magnetic stirring at room temperature. Then 20 mL of chitosan solution was diluted with the addition of 20 mL of methanol. AgNO_3 crystal (0.1800 g) was weighed in a weighting-boat, and then it was transferred slowly into a 100 mL three-neck-round bottom flask under magnetic stirring. The weighting boat was rinsed with a few drops of distilled water. During AgNO_3 dissolution, the flask was wrapped with aluminum foil to avoid direct contact with sunlight. The round flask was connected with a thermometer, rubber stopper, and a Liebig condenser and placed within a water bath. A Tungsten lamp (40 W) was placed 5 cm distance from the solution, and it was turned on to irradiate the solution for 90 min. The temperature solution might rise ~ 40 °C in a water bath. Two milliliters of the solution were sampled to follow the color change from colorless to brown, indicating the formation of AgNPs. The absorbance of chi-AgNPs colloidal was recorded by using a UV-Vis spectrophotometer at 400–700 nm.

2.3. Coating and characterization of chitosan-coated white-silica-gel beads (chi-SiG)

Coating procedure was prepared according to a previously described protocol (Adlim et al., 2021) with some modifications. White-silica-gel beads (28.8660 g) were soaked within 50 mL of chitosan solution (as prepared in Section 2.2) for 60 min at room temperature, then it was dried into the oven for 60 min at 40 °C (called the first coating) and denoted as chi-SiG. Next, the chi-SiG was soaked again within 50 mL of chitosan solution for 60 min at room temperature and dried into an oven for 60 min at 40 °C (as the second coating), then it was repeated until the third coating. The drying process was carried out until a constant weight was attained. Each step of the coating was characterized by using binocular microscope stereo and SEM. The three-time coated chi-SiG was then used further in the following experiments.

The coating stability of chi-SiG was tested by suspending the chi-SiG into several solvents, which were 1.5% (v/v) aqueous acetic acid, distilled water, and methanol. In a separated small beaker, every two granules of chi-SiG were soaked into 5 mL of 1.5% (v/v) aqueous acetic acid, 5 mL of distilled water, and 5 mL methanol for 60 min at room temperature. The chi-SiG was then dried in the oven for 30 min at 40 °C. The chi-SiG was observed using a binocular microscope stereo.

The swelling property of chi-SiG was studied by soaking each dried chi-SiG (3 granules) into each following solvents; 1.5% (v/v) aqueous acetic acid, distilled water, and methanol for 60 min. The different weights of dried chi-SiG and wet chi-SiG were recorded with an analytical balance (dried sample as M_0 & wet sample as M_1). The wet chi-SiG piece was air-dried and dried in the oven until the constant weight and was denoted as M_2 . The swelling studies were referred to the previous report (Wu et al., 2018) with minor modifications.

Swelling properties (W_{sp} %) was calculated by using this equation:

$$W_{sp} = \frac{M_1 - M_0}{M_1} \times 100\% \quad (1)$$

Chitosan solubility (W_{cs} %) was calculated by using the equation:

$$W_{cs} = \frac{M_0 - M_2}{M_0} \times 100\% \quad (2)$$

W_{sp} (%) = Swelling property

W_{cs} (%) = Chitosan solubility

M_0 = weight of the dried sample before immersing into the solvent

M_1 = weight of the wet sample after immersing into the solvent

M_2 = weight of the dried sample after immersing into the solvent

2.4. Immobilization and characterization of AgNPs on chi-SiG to form AgNPs-[chi-SiG]

Immobilizing AgNPs on chi-SiG followed a previous study (Hidayat et al., 2021). The chitosan layer on chi-SiG was used as the template and stabilizer for AgNPs in the immobilization process. The chi-SiG (28.866 g ~ 902 granules) was placed into

a 100 mL round flask, then 20 mL of methanol containing 0.18 g of $AgNO_3$ was added. Methanol containing $AgNO_3$ was covered with aluminum foil to avoid sunlight contact. The flask was set in a rotary evaporator and rotated at 200 rpm, equipped with a water bath without heating. While rotating, the Tungsten lamp (40 W, at 5 cm distance from the round flask) irradiated the round flask for 90 min, and the temperature was maintained at ~ 40 °C. The chi-SiG color changed from colorless to faintly red-brownish, indicating the formation of AgNPs on chi-SiG and was denoted as AgNPs-[chi-SiG]. AgNPs-[chi-SiG] was dried by heating until it reached the constant weight. The surface morphology of AgNPs-[chi-SiG] was characterized using a binocular microscope stereo and SEM. Then the AgNPs particle size on the surface of chi-SiG was analyzed using TEM. Five granules of AgNPs-[chi-SiG] was suspended into distilled water for 24 h, then shaken to pile off the outer film containing AgNPs. The slurry was recorded using TEM according to the previous method (Adlim et al., 2004).

The amount of silver attached to the ch-SiG was determined by using the AAS method. AgNPs-[chi-SiG] (4.9650 g) was transferred into a 250 mL beaker, and 5 mL of concentrated HNO_3 was added. The solution was mixed for 10 min by using a glass spatula. Then, distilled water (100 mL) was added and mixed thoroughly. The mixture was boiled until the volume was ~ 30 mL to expel nitric acid digestion gases and dissolve all soluble salts. The solution was then filtered with a Whatman filter paper (#2) into a 50 mL volumetric flask. The distilled water was added to rinse the filter paper up to 50 mL before AAS analysis.

2.5. Antibacterial property of AgNPs-[chi-SiG] against Gram-positive and Gram-negative bacteria

The antibacterial test was performed by a previous study (Hidayat et al., 2021). AgNPs-[chi-SiG] antibacterial properties were tested against *S. aureus* (Gram-positive) and *E. coli* (Gram-negative) by determining the inhibition zone diameters after exposure to the samples. We used chi-SiG and white-silica-gel as the control. Bacterial suspension used was 0.5 McFarland standard equal to 1.5×10^8 CFU/mL bacteria and inoculated on an agar plate of Mueller-Hinton Agar (MHA). Three granules (AgNPs-[chi-SiG]) were put into a petri dish that contained MHA and bacterial suspensions. Similar procedures were repeated for white-silica-gel beads as control and chi-SiG. The agar plate was then incubated at 37 °C for 24 h before measuring the inhibition zone diameters.

2.6. Preparation of air-filter containing AgNPs-[chi-SiG] and simulated-air-filter media

Air-filter was made from pieces of acrylic glass with a length of 14 cm, a width of 10.5 cm, and a thickness of 2 mm (Fig. 1). This air-filter was coated with a plain tile cloth (14 cm × 10.5 cm) which has a pore size of ± 1 mm to cover all sample granules in the filter, then the prepared AgNPs-[chi-SiG] (29.470 g) was filled into this air-filter. The filter containing the AgNPs-[chi-SiG] granules was prepared in two conditions that are dried and wet conditions. The AgNPs-[chi-SiG] were sprayed with distilled water before being inserted in the air-filter chamber (Fig. 2). This treatment was noted as a wet con-

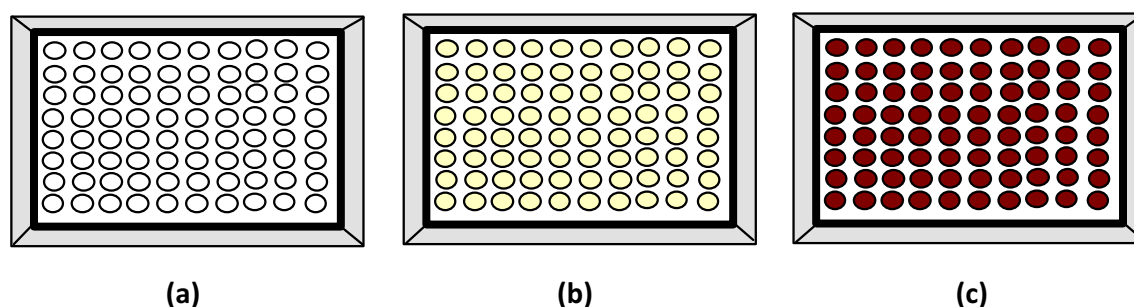


Fig. 1 Air-filter containing (a) SiG, (b) chi-SiG, and (c) AgNPs-[chi-SiG].

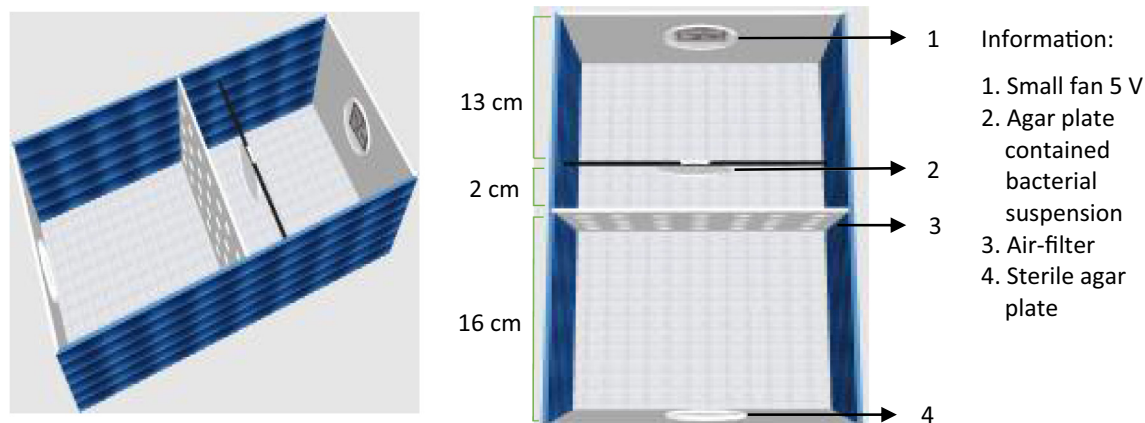


Fig. 2 Simulated-air-filter media.

dition. Air-filter containing chi-SiG and SiG (as control) were also prepared for control of antibacterial test, as shown in Fig. 1. Each air filter was a single layer containing 902 granules.

The simulated-air-filter chamber was made from acrylic glass (31 cm × 15 cm × 11 cm) and equipped with a 5 V small fan (8.8 cm × 9 cm × 3.7 cm). The chamber was in a vertical position, and the fan was placed at the top. Both air filter, the chamber media was sterilized using UV light irradiation (ESCO Airstream) at 250 nm for 30 min. Two agar media were prepared; one sterile (at the bottom) and the other contained bacterial suspension (on the top), as presented in Fig. 2. The fan was turned on to dry and to flow media containing bacteria. The air-containing bacteria passed through the air filter. The experiment was performed for two days, and the fan was run for 60 min per day at a velocity of 3.1 m/s. The bacteria colony before and after filtering was compared, and bacteria stuck on the sterile agar plate was also observed. The detailed procedure for the bacterial test is described in Section 2.7.

2.7. Antibacterial property of air-filter containing AgNPs-[chi-SiG]

The bacterial suspension (1 McFarland standard, which is equal to 3×10^8 CFU/mL bacteria) was inoculated on an agar plate of Nutrient Agar (NA) and inserted into the air filter chamber. Air-filter containing dried AgNPs-[chi-SiG] was inserted in between *B. subtilis* agar media and the sterile agar media. The media was then incubated at 35 °C for 48 h, and

the air was flown from *B. subtilis* agar media to penetrate AgNPs-[chi-SiG]. Within the air-filter compartment, a small fan blew air slowly in the surface agar plate containing *B. subtilis* bacteria. The agar plate slowly dried, and *B. subtilis* produced the spores (Franklin & Clark, 1981). The passing air containing bacterium spores were flown into sterile agar media. Then, the number of bacteria colonies before and after penetrating the air filter was compared. The experiment was repeated after 24 h and 48 h incubation in the chamber. The colonies were counted by using colony counter (BISQUIT Industrial Co.) Similar procedures were carried out for air-filter containing wet AgNPs-[chi-SiG], air-filter containing chi-SiG, and air-filter containing SiG (as control) tested against *B. subtilis*. The bacteria staining procedure was conducted according to the Gram staining protocol (Gerhardt, 1981). The steps involved the fixation and staining using safranin. If staining gives blue/purple, then the *B. subtilis* exists. The spore staining procedure was followed the Schaeffer-Fulton method by using a malachite green stain, and after the spore stain, the oval spores stained would be green, and the long vegetative cells stained would be red–orange. Both Gram and spore staining were observed through a microscope.

2.8. Characterizations

UV–visible (UV–Vis) absorption spectra of the chi-AgNPs colloidal were registered using a UV–Vis spectrophotometer (Shimadzu UVmini-1240, Indonesia). Fourier-transform infrared spectroscopy (FTIR, Shimadzu IRPrestige-21, Indonesia) was used to analyze the bonding of synthesized nanoparticles

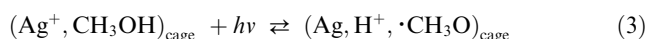
with functional groups of chitosan. Binocular microscope stereo (Olympus SZ61, Indonesia) equipped with an optical camera (OptiLab, Indonesia) was used to observe SiG, chi-SiG (original, before, and after immersing with solvents), and AgNPs-[chi-SiG]. The energy dispersive X-Ray spectroscopy (EDS) was carried out on a scanning electron microscope (SEM, JEOL JSM 6360 LA, Indonesia). Ag^+ content on AgNPs-[chi-SiG] was detected by atomic absorption spectroscopy (AAS, iCE 3000 SERIES, Indonesia). Philip CM 12 transmission electron microscope (TEM) was used to evaluate the size and shape of AgNPs on AgNPs-[chi-SiG]. The sample was prepared according to the previous report (Adlim et al., 2004). Spore and Gram staining were observed under a microscope (Olympus CX-21, Indonesia).

3. Result and discussion

3.1. Preparation and characterization of colloidal chi-AgNPs

Before immobilization of AgNPs in the air filter, the formation of chi-AgNPs was studied from the colloidal phase. Silver ions formed coordination bondings with amino groups ($-\text{NH}_2$), providing lone pair electrons in chitosan chains. Chitosan also contains lone pair electrons from $-\text{OH}$. Ag^+ , as soft acid, preferred to bond with a softer base like N (65 pm of atomic radius) instead of forming bonding with O (60 pm of atomic radius). Distributing silver ion with chitosan matrix before reduction to silver metal proposed to disperse silver metal colloidal particles.

The silver ion photoreduction mechanism in methanol has been described in previous study (Hada et al., 1976). The electrons from methanol (CH_3OH) move to silver ions in the presence of photons. Silver ions are surrounded with CH_3OH molecules noted as a cage. CH_3OH transfer e^- to Ag^+ and formed Ag, proton and $\cdot\text{CH}_3\text{O}$ radicals



Then solvent cage gradually decomposed



The methoxy radicals ($\cdot\text{CH}_3\text{O}$) transfer the electron into other Ag^+ to form methanal.



The redox reaction is thermodynamically feasible since they have large different reduction potentials, that are $\text{HCHO}/\text{CH}_3\text{OH}$ ($E^\circ_{\text{red}} = \sim -0.45$ V, SHE) and Ag^+/Ag ($E^\circ_{\text{red}} = +0.8$ V, SHE). Trace of CH_3OH and HCHO were all evaporated off at room temperature since they were volatile with the boiling point of 64.7 °C and -19 °C, respectively.

During irradiation, the UV-Vis spectra of the colloidal chi-AgNPs were periodically recorded, and the spectra reached a maximum after 70 min of irradiation, as presented in Fig. 3 (a). The spectra gradually shifted to a higher wavelength until a maximum at 580 nm as the plasmon band. According to the previous adsorption spectra study on large colloidal silver colloid in water (Sukhov et al., 1997), the spectra shift might indicate the reducing completion of Ag^+ reached nearly maximum ($\sim 90\%$) and enlarging Ag colloidal particles (20–30 nm). The UV-Vis absorption spectra exhibited broader absorbance in 60–70 min synthesis time, and the higher absorbance indicated the greater yield AgNPs. Reduction time also confirmed the previous studies that found after 60 min irradiation, the colloidal Ag spectra nearly maximum intensity (Harada & Katagiri, 2010). The shifting to a longer wavelength might indicate the agglomeration of colloidal silver particle size by reduction time (Paramelle et al., 2014). However, other factors, including the stabilizer, reducing agent/technique, might affect the UV-Vis spectra properties of colloidal AgNPs (De Leersnyder et al., 2020). The agglomeration formation might be explained by studies conducted by Harada & Katagiri (2010).

However, these typical chi-AgNPs colloidal absorbance spectra were consistent with the literature (Matsumoto et al., 2006; Ifuku et al., 2015). The consequent color changes were observed from colorless to brown, indicating the production of AgNPs during the reaction (Zielinska et al., 2009). The spectra were broad and shifted to a higher wavelength along with irradiation time. The maximum absorbance around 550–590 nm is comparable with the previous report, especially when the chi-AgNPs had changed to brown (Ifuku et al., 2015). Other findings reported the maximum spectra of chi-AgNPs were between 400 and 500 nm, which is related to the yellowish color (Adlim, 2006a; Adlim et al., 2021). The chi-AgNPs brown color and broad spectra might indicate par-

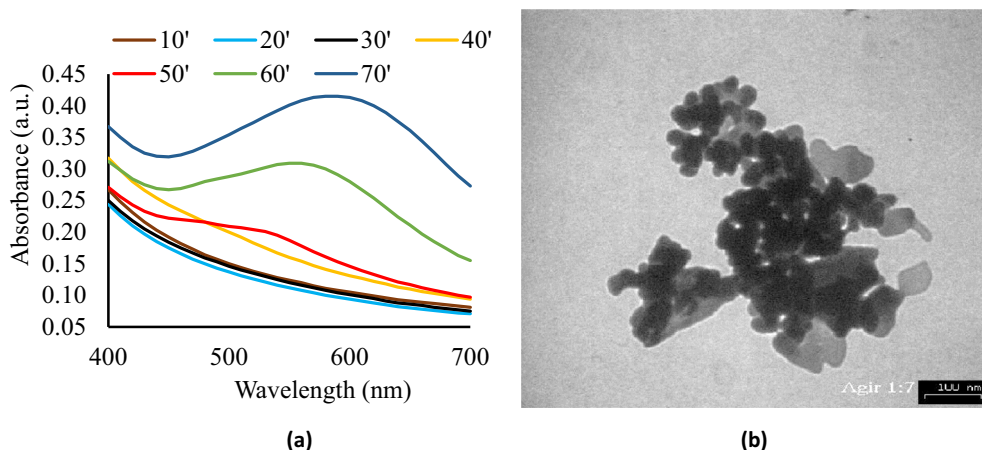


Fig. 3 (a) UV-Vis spectra of chi-AgNPs colloidal, and (b) TEM image of AgNPs colloidal (scale bar = 100 nm).

ticle agglomeration, especially after one week of storage. This is consistent with an earlier report (Adlim, 2006a). The particle aggregation of colloidal chi-AgNPs in this current study was confirmed with TEM image, as shown in Fig. 3(b). TEM analysis revealed that in 70 min of synthesis time, spherical and mixed morphology (bars and rods) AgNPs within clusters were formed and showed that chi-AgNPs particles were aggregated with the mean particle size of 8.5 ± 4.1 nm (Fig. 3b). In some literature, the particle size of colloidal chi-AgNPs was in arrange of 4–120 nm (Adlim, 2006a; Chen et al., 2019; Zong et al., 2014). Thus, the preparation of chi-AgNPs in the presence of methanol by visible light photo-irradiation gave colloidal AgNPs, and the particle started to aggregate after one week of storage. Rapid nucleation process of particles with a diameter of ~ 2.5 nm might occur during irradiation time, then Ostwald ripening growth for bigger aggregation (~ 11.5 nm) and finally dynamic coalescence of large growth particles (Harada & Katagiri, 2010). Due to considerable energy, the AgNPs tend to agglomerate leading to a decrease in antibacterial potential, which can be solved by loading AgNPs on a solid support (Nie et al., 2018) as a promising strategy for synthesis uniformly distributed functionalized AgNPs and it is described in Section 3.3. The physical properties like size, shape, and uniform distribution are vital properties that impact the antibacterial action of AgNPs. As far as shape and size are concerned, it has been found that smaller nanoparticles and well distributing are more stable and display a higher antimicrobial activity (Li et al., 2013).

The chitosan stabilizing properties towards colloidal AgNPs were related to electron pairs of $-\text{OH}$ and $-\text{NH}_2$ groups within chitosan chains that interact with Ag^+ prior to the chemical reduction process (Hang et al., 2010; Huang et al., 2004; Reicha et al., 2012; Twu et al., 2008). We attempted to prove the interaction by FTIR method, but the specific band was not very noticeable, as shown in Fig. 4.

The observed band at 3401.61 cm^{-1} (chitosan) was shifted to 3424.76 cm^{-1} (chi-AgNPs) and is ascribed to the valence vibrations (stretching) of $\text{O}-\text{H}$ and $\text{N}-\text{H}$ intramolecular hydrogen bonds (Ghaseminezhad et al., 2012; Senthilkumar et al., 2017) which reflected the presence of interactions between Ag, and N atoms of $-\text{NH}_2$ groups. The band alter-

ation is comparable to previous reports on chitosan-AgNPs (Nate et al., 2018; Dara et al., 2020).

3.2. Coating and characterization of chitosan-coated white-silica-gel beads (chi-SiG)

We learned from our previous work that simultaneous preparation of colloidal-metal-nanoparticles and the immobilization process (in-situ process) on the solid support was not preferable. We found that when chitosan film covered up the surface metal-nanoparticles this subsequently caused the AgNPs to be less accessible and had low catalytic activity (Adlim, 2006b). Therefore, the white-silica-gel beads (SiG) were prepared by coating with chitosan film to enhance the surface stickiness and provide sites for Ag^+ prior to the immobilization of AgNPs. By which, AgNPs were dispersed and stabilized.

Three layers of chitosan coating on SiG were observed using binocular microscope stereo and SEM. The microscope images of SiG (control) and chi-SiG are displayed in Fig. 5. The chitosan film was very thin ($12.24\text{--}57.14\text{ }\mu\text{m}$) and transparent yellowish, and it surrounded the SiG surface (Fig. 5b). At higher magnification, the chitosan film surface on SiG looks wrinkled (Fig. 5c), while the SiG surface was smooth (Fig. 5a).

A closer appearance of the chitosan layer is presented in the SEM pictures (Fig. 6). The surface morphology at low magnification ($500\times$) showed several thin layers of chitosan film wrapped around the surface of SiG (it is shown by the red arrows in Fig. 6a). This is consistent with the preparation process where SiG was coated with three layers of chitosan film. At higher magnification ($5000\times$), the chitosan microfibril, with a diameter of approximately $5\text{ }\mu\text{m}$ covering the SiG surface, can be observed in detail (as shown by the red arrows in Fig. 6b). The existence and morphology of chitosan layers confirmed an appropriate template for the incorporation of AgNPs. Further confirmation of chitosan-coated SiG was achieved using EDS analysis that the presence of 27.02 mass % carbon was contributed from chitosan polymers, and Si was from silica beads.

The dried-chitosan layer on chi-SiG was immersed into the various solvents to investigate the extent to which the dried-

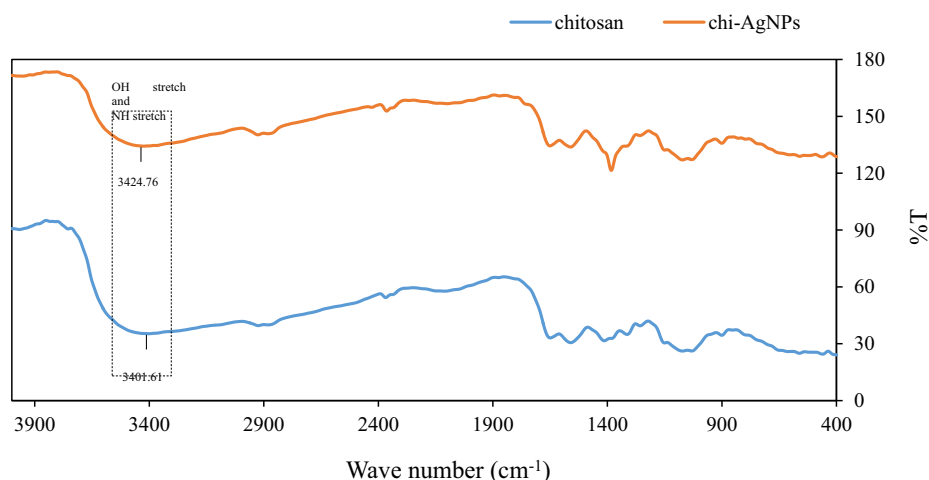


Fig. 4 FTIR spectra of chitosan and chi-AgNPs.

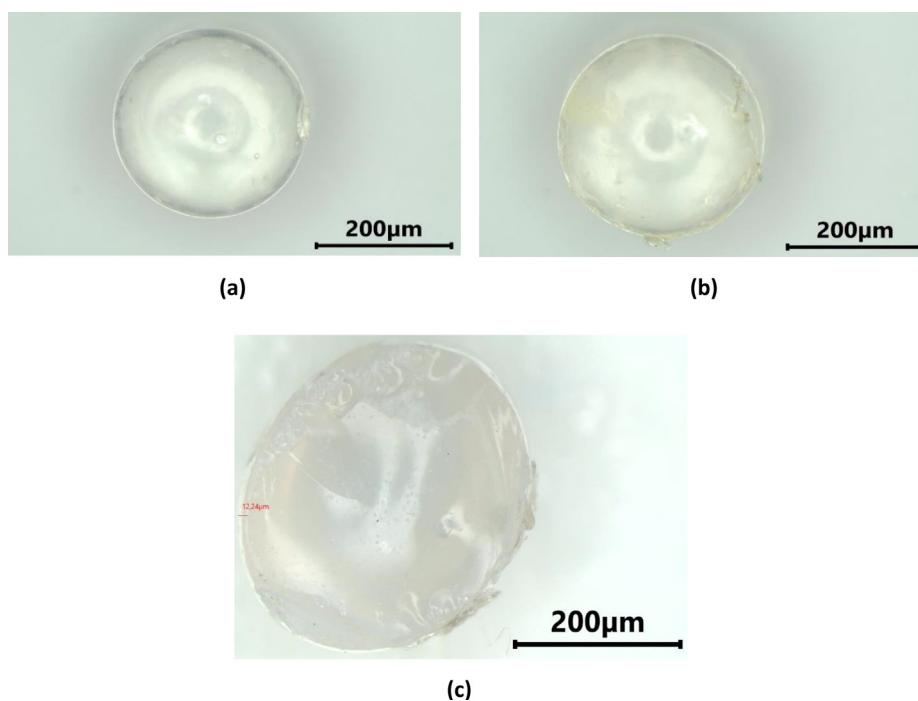


Fig. 5 Microscope images of cross-section of (a) SiG with $13 \times$ magnification, (b) chi-SiG with $13 \times$ magnification, and (c) chi-SiG with $20 \times$ magnification.

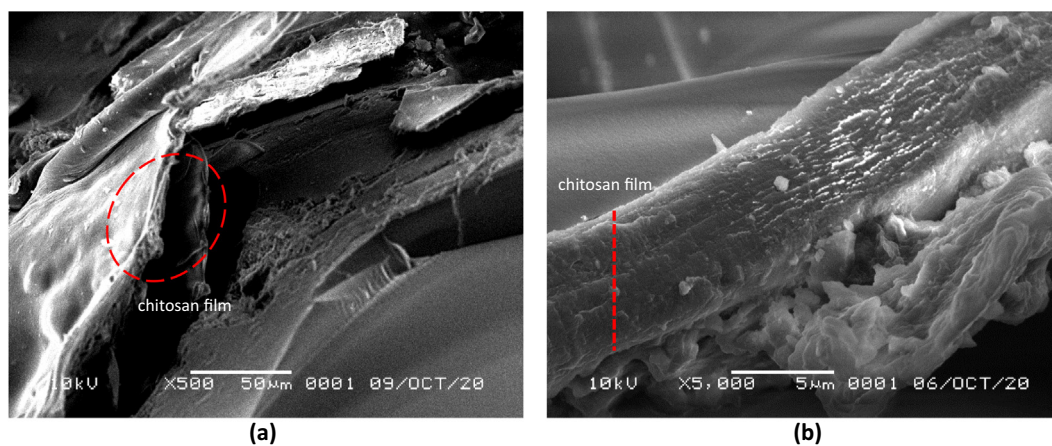


Fig. 6 SEM images of chi-SiG with (a) $500 \times$ magnification, and (b) $5000 \times$ magnification.

chitosan layer is stable. Microscope images of the chi-SiG after immersion in methanol, distilled water, and 1.5% (v/v) acetic acid are displayed in Table 1. Table 1 showed that compared to control and the other solvents (distilled water and acetic acid), methanol destroyed the coating less and became the appropriate solvent for immobilization of chi-AgNPs.

The coating stability was confirmed from the swelling test of chi-SiG, as presented in Table 2. Table 2 showed that all the solvents caused chi-SiG to swell with swelling properties of 5.23 ± 2.8 , 31.50 ± 14.0 , and 18.87 ± 9.4 for methanol, distilled water, diluted-acetic acid, respectively. The chi-SiG swelled excessively in distilled water, and chi-SiG swelled and destroyed the chitosan coating in a diluted acetic acid solvent. Only 30.3% of the chitosan coating remained, while the rest dissolved (weight loss) in the acetic acid (Pardo-Castaño and

Bolaños, 2019). The swelling is less in methanol, only 2.32–7.83% and no chitosan dissolution occurred, consistent with the microscope images shown in Table 1. Hence, methanol did not destroy the chitosan coat. Therefore, methanol was chosen as the solvent for the immobilization process. This finding is consistent with the previous report (Hidayat et al., 2021).

3.3. Immobilization and characterization AgNPs on chi-SiG to form AgNPs-[chi-SiG]

Immobilization of AgNPs on chi-SiG, which is then symbolized as AgNPs-[chi-SiG] was evaluated by observing the surface through SEM, and the particle size was evaluated by TEM. The SEM images of AgNPs-[chi-SiG] presented in Fig. 7 show that the surface was different from chi-SiG both

Table 1 Observation results of immersion chi-SiG in various solvents through binocular microscope stereo with 13 × magnification.

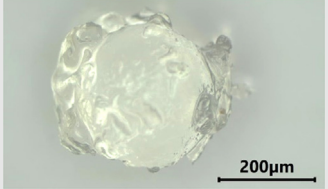
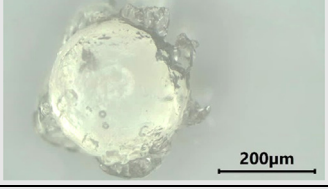
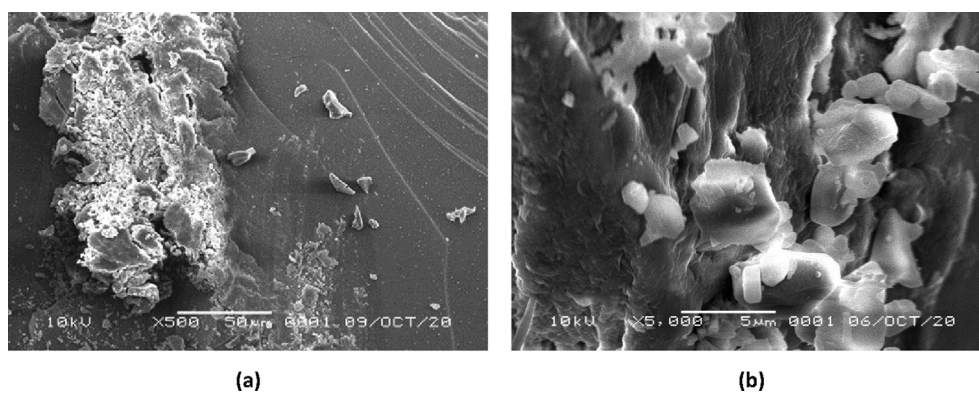
Solvent	Before immersion	After immersion
Methanol		
Distilled water		
1.5% (v/v) acetic acid		

Table 2 The results of swelling property and chitosan solubility in various solvents using gravimetric method.

Solvent	No.	M ₀ (g)	M ₁ (g)	M ₂ (g)	W _{sw} (%)	W _{cs} (%)	Chi loss (wt%)
Methanol	1	0.047	0.051	0.047	7.84	-	0
	2	0.034	0.036	0.034	5.55	-	0
	3	0.042	0.043	0.042	2.32	-	0
				mean	5.23 ± 2.8		
Distilled water	1	0.055	0.081	0.055	47.27	-	0
	2	0.030	0.041	0.030	26.83	-	0
	3	0.039	0.049	0.039	20.41	-	0
				mean	31.50 ± 14.0		
1.5% (v/v) acetic acid	1	0.033	0.046	0.032	28.26	30.30	69.7
	2	0.030	0.037	0.029	18.92	30.30	69.7
	3	0.053	0.058	0.052	9.43	30.30	69.7
				mean	18.87 ± 9.4		

**Fig. 7** SEM images of AgNPs-[chi-SiG] with (a) 500 × magnification, and (b) 5000 × magnification.

at low and high magnification (Fig. 6). Fig. 7(b) showed the number of white aggregates with a size of $\sim 1\text{--}3\ \mu\text{m}$ that might represent of AgNPs assemble. The aggregates are contrasting from the chitosan layer (Fig. 8b). Immobilized AgNPs on chi-SiG to form AgNPs-[chi-SiG] was confirmed.

After immersing AgNPs-[chi-SiG], the slurry was analyzed by TEM measurement, and the represented image is shown in Fig. 8(a). The TEM image of AgNPs of AgNPs-[chi-SiG] was different from the colloidal chi-AgNPs (Fig. 1a). Unlike the colloidal nanoparticles, TEM analysis revealed uniformly spherical AgNPs with fine dispersion (Fig. 8a) and slightly larger particles with a diameter mean of $13.18 \pm 6.9\ \text{nm}$ (Fig. 8b). It is worth understanding that the antibacterial efficiency of AgNPs is strongly influenced by their stabilization on given support. The stabilizer prevents particles from agglomeration, which affects the biocidal activity. This study confirmed that AgNPs on chi-SiG are stable without precipitation, dispersed particles without excessive aggregation. The stability is related to the chitosan role in the composite (Ranjani et al., 2019). The different sizes and shapes might correlate with the immobilization technique. AgNPs in colloidal (chi-AgNPs) was inside of chitosan matrix, and all AgNP surfaces were covered with chitosan solution. The different phenomenon occurs in AgNPs-[chi-SiG] sample. The Ag ions were previously impregnated on the surface of the [chi-SiG] (solid), then Ag ions were subsequently reduced to form silver metal nanoparticles (AgNPs). Such sequence preparation makes AgNP surface assessable for bacteria interaction. This finding verified the previous study of immobilization of chi-Pd/Au on titania (Adlim & Bakar, 2013). Therefore, this stepwise-immobilization technique was confirmed as the appropriate method. This solid system also promises several advantages, including compatibility on separation, regeneration, storage, and lower cost. According to AAS data, the mean of silver weight in each granular of AgNPs-[chi-SiG] was 0.0135 mg or 0.4028 mg per gram of AgNPs-[chi-SiG] granular.

3.4. Antibacterial property of AgNPs-[chi-SiG] against Gram-positive and Gram-negative bacteria

Before AgNPs-[chi-SiG] granules were assembled as an air filter, the antibacterial properties of AgNPs-[chi-SiG] granules, chi-SiG and SiG as the control were studied against *S. aureus* and *E. coli* bacteria. As shown in Fig. 9, all samples exhibit an inhibition zone against both types of bacteria except SiG without chitosan coating. The chitosan content in chi-SiG caused chi-SiG to have antibacterial properties, but the number of chitosan layers did affect, as shown in Table 3. The chi-SiG seems to have higher antibacterial properties than AgNPs-[chi-SiG]. This might be related to the hydrophilic effect. Chitosan layer swells in water (agar system), then antibacterial effect diffused easily. In the case of AgNPs-[chi-SiG], the low hydrophilicity of AgNPs-[chi-SiG] might be retard the effect in agar media. The antibacterial properties would not diffuse as easily in the agar system and subsequently have less effect on the bacteria. Therefore, AgNPs-[chi-SiG] was not significantly different from only chitosan content. The AgNPs content in the experiment was very low ($\leq 0.04\ \text{mg}$), and AgNPs are insoluble in water. The inhibition zone diameter of AgNPs-[chi-SiG] against *S. aureus* and *E. coli* were 15.40 mm and 14.38 mm, respectively.

The effect of chitosan on bacteria inhibition growth might be explained based on the interaction of the amino groups of chitosan with the bacteria cell wall. It would increase cell membrane penetrability that caused intracellular components to leak, disrupting respiration and preventing nutrients from entering the cell wall (Chien et al., 2016; Chang et al., 2019). Chitosan could cause the rupture of the cell membrane (Wang et al., 2021). However, some studies reported that neat chitosan film might not be effective over a longer period. Their surface tends to saturate with dead bacteria cells and lose their inhibition activity (Ardila et al., 2017).

Some reports indicated that silver with a spherical shape of silver nanostructure exhibited high antibacterial effectiveness against Gram-positive and Gram-negative bacteria

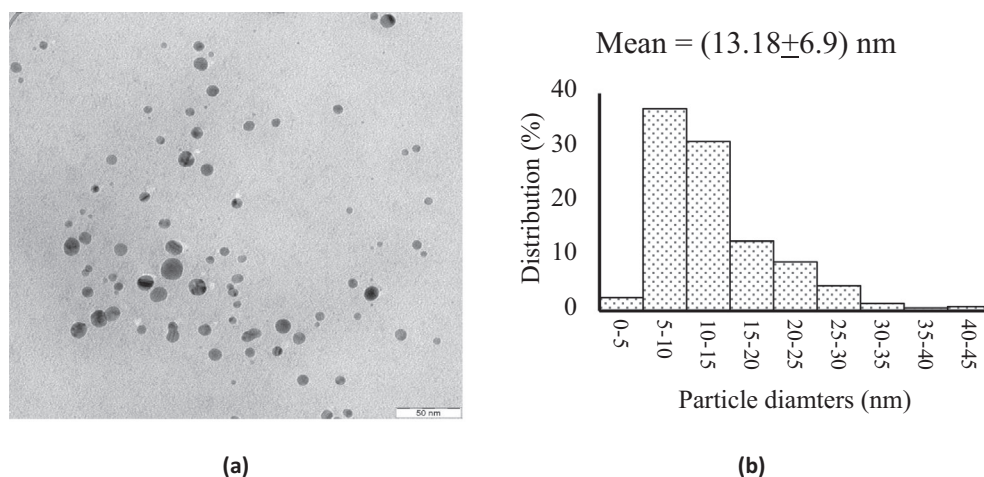


Fig. 8 TEM analysis (a) image of AgNPs (scale bar = 50 nm), and (b) particles size distribution of AgNPs.

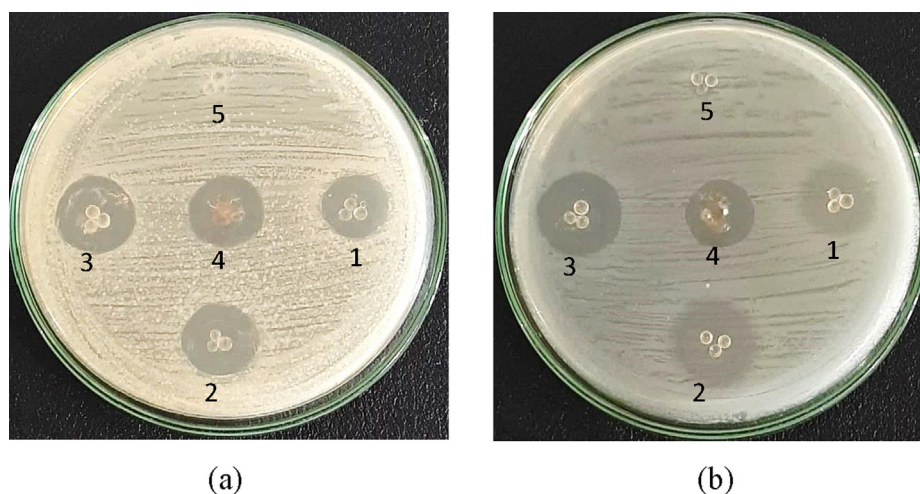


Fig. 9 Inhibition zone of chi-SiG tested against (a) *S. aureus* (b) *E. coli*; (1) chi-SiG coating 1 ×, (2) chi-SiG coating 2 ×, (3) chi-SiG coating 3 ×, (4) AgNPs-[chi-SiG], and (5) SiG (control).

Table 3 Inhibition zone diameter of prepared materials against Gram-positive (*S. aureus*) and Gram-negative (*E. coli*) bacteria.

Bacteria	Material	Inhibition zone diameter (mm) (mean ± SD)
<i>Staphylococcus aureus</i>	chi-SiG coating 1 x	14.35 ± 0.12
	chi-SiG coating 2 x	15.45 ± 0.24
	chi-SiG coating 3 x	16.70 ± 0.29
	AgNPs-[chi-SiG]	15.40 ± 0.37
	SiG as control	-
<i>Escherichia coli</i>	chi-SiG coating 1 x	13.50 ± 0.48
	chi-SiG coating 2 x	15.14 ± 0.02
	chi-SiG coating 3 x	16.43 ± 0.09
	AgNPs-[chi-SiG]	14.38 ± 0.06
	SiG as control	-

All experiments were performed in triplicates and reported as mean ± standard deviation (SD).

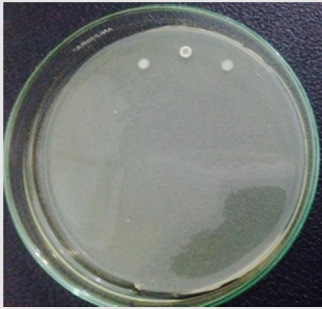
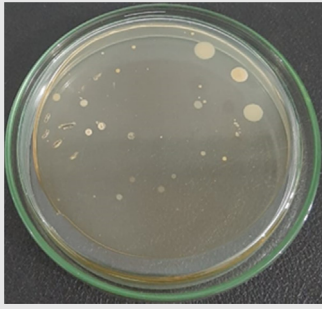
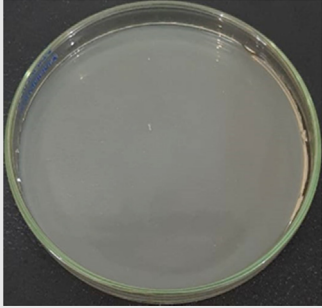
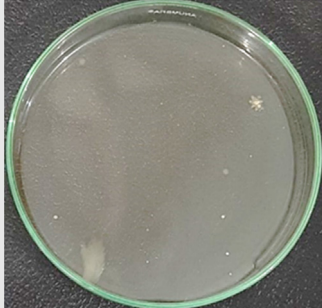
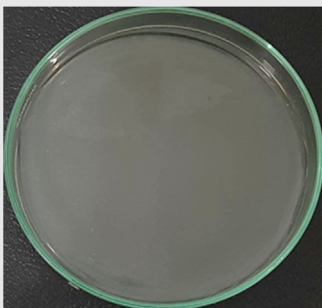
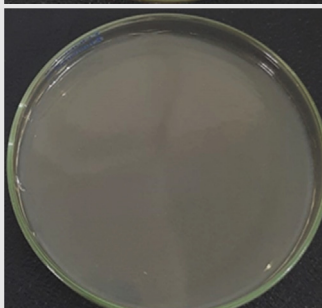
Table 4 Observation results of colonies using a colony counter for all filters.

Filter	The number of initial colonies (before filter penetration)	Incubation time (h)	The number of final colonies (after penetration)	Inactivation rate (%)
SiG	373	24	8	97
		48	52	86
chi-SiG	325	24	1	99.7
		48	15	95.4
AgNPs-[chi-SiG]	339	24	0	100
		48	4	98.8
AgNPs-[chi-SiG] contained 1.027% water	361	24	0	100
		48	0	100

(Ashkarran et al., 2013; Agnihotri et al., 2014; El-Zahry et al., 2015), so this is reasonable to use the synthesized AgNPs-[chi-SiG]. Due to the high surface to volume ratio, the smaller-sized nanoparticles released more silver cations and, thus, proved more effective in killing bacteria than larger-sized particles. The smaller spherical AgNPs showed good inhibitory action because a significantly large surface area was in contact with

the bacterial effluent compared to larger spherical AgNPs (Raza et al., 2016). When AgNPs are delivered as antibacterial, they get oxidized and release the Ag^+ ion responsible for the microbe's death. It is known that bulk silver metal has high reduction potential ($E^\circ \text{Ag}^+/\text{Ag} = +0.8$ Volt), indicating inert enough for oxidation, but the nano-size silver metal performs inversely. The AgNPs (Ag^0) is slowly oxidized to Ag^+ . The

Table 5 Images of colonies observation after through the filters.

Filter contents	Incubation time (24 h)	Incubation time (48 h)
SiG		
chi-SiG		
AgNPs-[chi-SiG] (dried)		
AgNPs-[chi-SiG] (wet) contained 1.027% water		

antibacterial effect is related to the interaction of AgNPs with sulphur-containing proteins in the bacteria cell membrane. AgNPs would infiltrate the cell interior and disrupt its normal metabolism (Duran et al., 2016). The difference in inhibition zone diameter between Gram-positive and Gram-negative bacteria (presented in Table 3) may be attributed to the antibacterial activity against *S. aureus*, which is superior to that of *E. coli* due to the difference in their cell wall structures. The cell walls of Gram-negative bacteria are multilayer structures, which contain a thin peptidoglycan layer, lipoprotein layer, phospholipids, or lipopolysaccharide layer. These complex layer structures weakened the interaction between chitosan/AgNPs and cells (Siripatrawan & Vitchayakitti, 2016). Meanwhile, the cell walls of Gram-positive bacteria are composed of

a thick but single peptidoglycan layer, so it easily interacts with chitosan/AgNPs. Therefore, a higher amount leaked through *S. aureus* membranes compared to those through the *E. coli* membranes, suggesting that the antibacterial sensitivity towards Gram-negative *E. coli* was lower than that of Gram-positive *S. aureus*, and this result was consistent with the previous studies (Xu et al., 2019; Cheng et al., 2019).

3.5. Antibacterial property of air-filter containing AgNPs-[chi-SiG]

Each of AgNPs-[chi-SiG], chi-SiG, and SiG granules were assembled to become a filter panel inserted in a simulated-air-filter chamber, as shown in Fig. 2. Since only *Bacillus sub-*

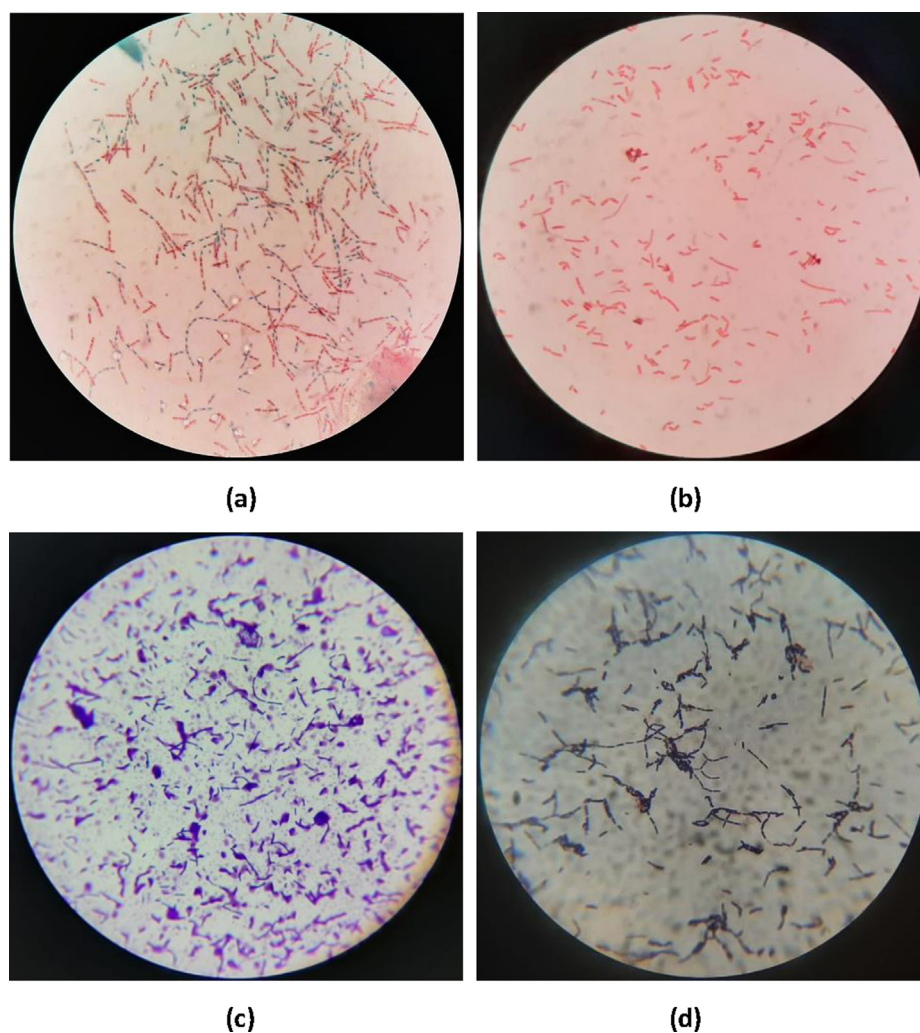


Fig. 10 Microscopic images of *B. subtilis* (a) spore stain after through SiG filter, (b) spore stain after through AgNPs-[chi-SiG] filter, (c) Gram stain after through SiG filter, and (d) Gram stain after through AgNPs-[chi-SiG] filter with $1.000 \times$ magnification using a microscope.

tilis produced spores flown in the air by a fan in the air-filter chamber, the experiment was limited to Gram-positive bacteria (Basta and Ammaraju, 2021). When the agar-petri-dish containing *B. subtilis* was blown by a small fan, then the humidity slowly decreased. Subsequently, *B. subtilis* became stressed and produced endospores that were flown to penetrate the filter (Errington, 2003).

The number of bacteria colonies before and after penetrating the AgNPs-[chi-SiG] filter panel were compared. The number of the colonies *Bacillus subtilis* is presented in Table 4. The microscope images of the colonies are presented in Table 5. Table 4 show several initial colonies (before penetration of the filter) were 372 colonies. The colony remained 8 and 52 after penetration of SiG filter during incubation of 24 and 48 h, respectively. Unlike in agar media test, AgNPs-[chi-SiG] show remain higher antibacterial properties than the chitosan coating only. The colony was reduced to 1 and 15 after penetration of chi-SiG filter during incubation time 24 and 48 h. The colony disappeared after penetrating the dried AgNPs-[chi-SiG] filter, although there were 4 colonies still existed after 48 h of incubation times. The air was sterile from

the bacteria after filtering with the wet AgNPs-[chi-SiG]. The strength of AgNPs was due to their higher bacteriostatic and bactericidal properties. Thereby, nanoparticles were trusted as a preventive agent for bacterial contamination in prolonging activity (Mathur et al., 2018; Angulo-Pineda et al., 2019; Khorrami et al., 2020).

Fig. 10 confirmed the existing flown-endospore, and the reduction of colony intensity was also verified after penetration of the filters. Fig. 10(a) showed many spores and vegetative cells after penetration of the SiG filter. Such morphology indicated that these cells were alive and metabolically active. The morphology was different after penetration of the AgNPs-[chi-SiG] filter. The spores were not found inside the vegetative cells (Fig. 10b). AgNPs might induce process sporulation in *B. subtilis* cells. The spore development depends on the expression and phosphorylation level of transcription factor and regulator Spo0A \sim P, which is responsible for the activation of subsequent sporulation genes (Eymard-Vernain et al., 2018). Based on the observation of spore staining, it can be hypothesized that the existence of AgNPs is necessary to stop the sporulation process by inhibiting protein synthesis. Fig. 10(c)

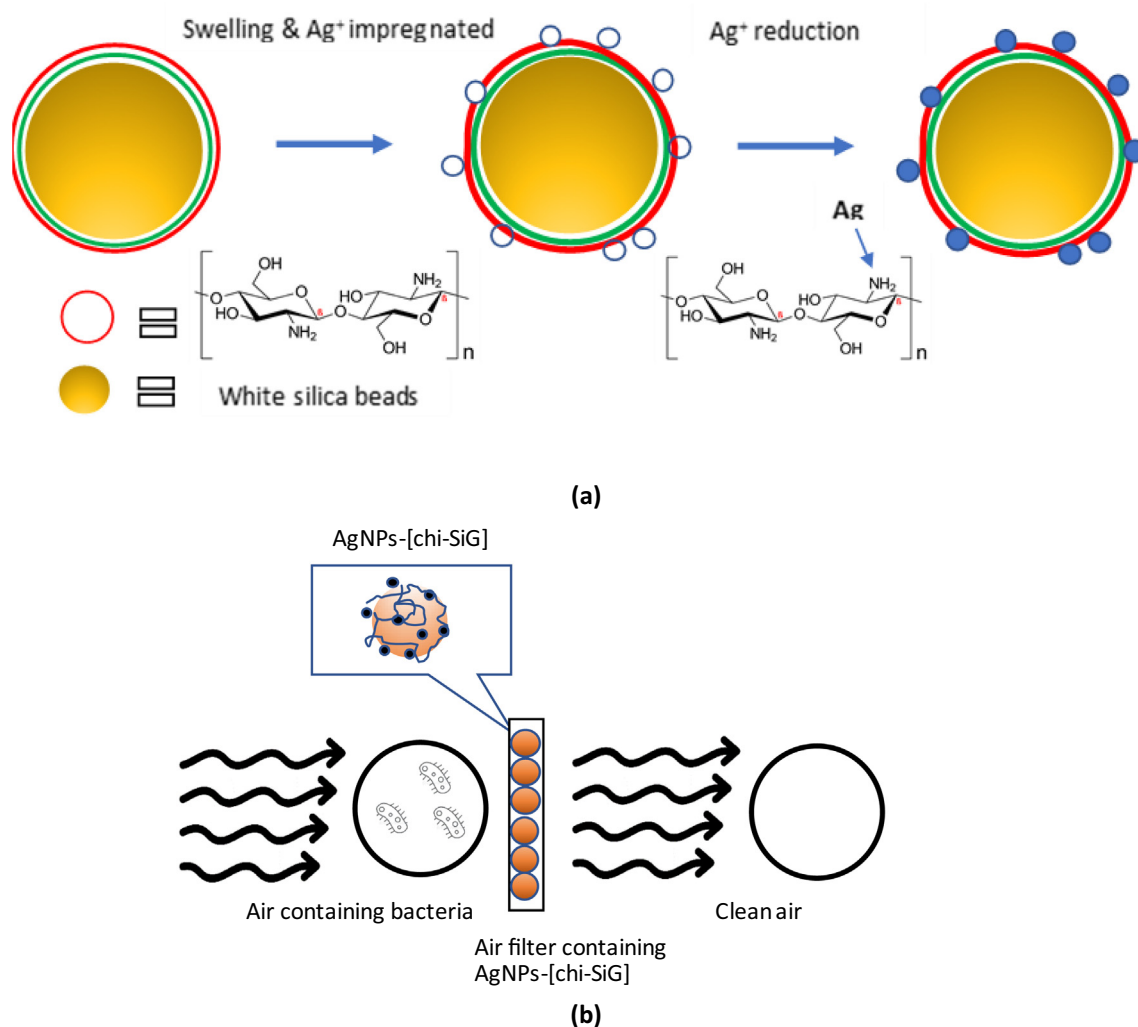


Fig. 11 (a) illustration of AgNPs-[chi-SiG] preparation; white-silica-gel beads coated with chitosan films, swelled chitosan films, impregnated silver ion and silver reduction, and (b) the graphical abstract of air filter containing AgNPs-[chi-SiG] and the antibacterial experimental set-up.

shows Gram staining of the existing colonies after entering the SiG filter. Some *B. subtilis* bacteria were still alive and had regular shapes (Fig. 10c). After filtering with the AgNPs-[chi-SiG] filter, the cells were shrunk and had an unusual color (Fig. 10d). These results confirmed AgNPs on the filter that acted as an antibacterial agent, so it is effective in reducing airborne bacteria. This finding is also consistent with previous studies on *B. subtilis* that showed AgNPs initiate the sporulation and also inhibit the cell growth of *B. subtilis* bacteria (Gambino et al., 2015; Rafińska et al., 2019). Although the mechanisms underlying the antibacterial actions of silver are still not fully understood, several previous reports showed that the interaction between silver and the constituents of the bacterial membranes cause structural changes and damage to the membranes and intracellular metabolic activity (Roy et al., 2019; Behzad et al., 2020).

Some studies have shown that smaller spheres AgNPs have been associated with increased antibacterial activity by the release of many Ag^+ (El-Zahry et al., 2015; Fan et al., 2021).

Using Ag^+ directly is not preferable due to excessive dissolution and early loss of bacterial activity (Korshed et al., 2018).

In contrast, the bulk silver metal is inert enough to release ion Ag^+ . AgNPs with slow-release Ag^+ shows effective antibacterial properties. Since AgNP is relatively expensive, then immobilizing it in silica gel beads gave several advantages. It will disperse AgNPs on the surface and stabilize AgNPs (Karunamuni et al., 2016). Also, it prevents airflow blockage when applied in an air filter. Chitosan/silica phase decorated by AgNPs has been reported to be an effective antibacterial application (Nie et al., 2018; Zienkiewicz-Strzałka et al., 2019; Abaza et al., 2021), but AgNPs are not immobilized in silica gel beads, and the synthesis took a long time and needed specific equipment. The present work established a simple, rapid, low-cost, and environmentally friendly synthesis of AgNPs-[chi-SiG]. As a template for nanoparticle attachment, chitosan coats on white-silica-gel beads can notably enhance the antibacterial activity of AgNPs. Chitosan functioned as the stabilizer (Kumar-Krishnan et al., 2015). Silica gel beads dispersed the silver metal particles on the surface and prevented airflow blockage in the air filter operation. Therefore, the AgNPs-[chi-SiG] investigation in the agar well diffusion method (against *S. aureus* and *E. coli*) and in the simulated-

air-filter (against *B. subtilis*) was effectively acted as antibacterial material. The coating of white-silica-gel beads with chitosan film, swelling of the chitosan films, the impregnating of silver ions on chitosan film, and the reducing of silver ions are illustrated in Fig. 11(a). The air filter model containing AgNPs-[chi-SiG] and the experimental set-up of antibacterial test in simulated polluted air are modelled in Fig. 11(b).

4. Conclusion

Preparation and immobilization of AgNPs on a solid support and the installation on antibacterial-air-filter were confirmed as the suitable procedure to give a compatible and green product with high antibacterial activity. The visible irradiation on chitosan containing silver ions in the presence of methanol was confirmed as the silver reduction technique for colloidal AgNPs. Methanol was easily removed by evaporation, and the rest were nonharmful materials. The stepwise immobilization method gave dispersed and nano-size silver metal (solid). The chitosan coat functioned well as the stabilizer and the adhesive for AgNPs. Both chi-SiG and AgNPs-[chi-SiG] inhibited the surface adhesion of both Gram-positive (*S. aureus*) and Gram-negative (*E. coli*) bacteria within agar media. Air filter containing AgNPs-[chi-SiG] showed high antibacterial performance against *B. subtilis* in air.

Declaration of Competing Interest

The authors declare that they have no known competing financial interests or personal relationships that could have appeared to influence the work reported in this paper.

Acknowledgment

This work was supported by the PMDSU Scholarship for Muhammad Iqbal Hidayat and Research fund from the Kementerian Pendidikan, Kebudayaan, Riset dan Teknologi, Republic of Indonesia (grant number 154/SP2H/LT/DPRM/2021, March 18, 2021); and the Research University Grant awarded by Universiti Sains Malaysia (grant number 1001/PKIMIA/8011071).

References

- Abaza, S.F., Elbially, N.S., Mohamed, N., 2021. Incorporating silver nanoshell-coated mesoporous silica nanoparticles improves physicochemical and antimicrobial properties of chitosan films. *Int. J. Biol. Macromol.* 189, 792–801. <https://doi.org/10.1016/j.ijbiomac.2021.08.161>.
- Adlim, A., 2006. Immobilizing chitosan-stabilized palladium nanoclusters on titanium dioxide and their catalytic hydrogenation properties. *J. Mat. Sains* 11, 125–133.
- Adlim, A., Bakar, M.A., 2008. Preparation of chitosan-gold nanoparticles: effect of reducing technique. *Indo. J. Chem.* 8, 184–188. [10.22146/ijc.21621](https://doi.org/10.22146/ijc.21621).
- Adlim, M., Bakar, M.A., 2013. The properties of Pd/Au bimetallic colloidal catalysts stabilized by chitosan and prepared by simultaneous and stepwise chemical reduction of the precursor ions. *Kinet. Catal.* 54, 586–596. <https://doi.org/10.7868/S0453881113050018>.
- Adlim, M., Bakar, M.A., Liew, K.Y., Ismail, J., 2004. Synthesis of chitosan-stabilized platinum and palladium nanoparticles and their hydrogenation activity. *J. Mol. Catal. A Chem.* 212, 141–149. <https://doi.org/10.1016/j.molcata.2003.08.012>.
- Adlim, M., Hidayat, M.I., Azmi, N., Ramayani, R.F.I., 2021. Preparation of Chitosan-Silver Nanoparticles Immobilized onto Pumice for Antibacterial Testing Against *Escherichia coli*. In: *Proceedings of the 2nd International Conference on Experimental and Computational Mechanics in Engineering*. Lect. Notes Mech. Eng., pp. 63–72. https://doi.org/10.1007/978-981-16-0736-3_7.
- Adlim, 2006. Preparation of chitosan-stabilized silver (Chi-Ag) nanoparticles using different reducing agents and techniques. *J. Sains dan Teknol.* 12, 185–191.
- Agnihotri, S., Mukherji, S., Mukherji, S., 2014. Size-controlled silver nanoparticles synthesized over the range 5–100 nm using the same protocol and their antibacterial efficacy. *RSC Adv.* 4, 3974–3983. <https://doi.org/10.1039/C3RA44507K>.
- Alamgholilo, H., Rostamnia, S., Pesyan, N.N., 2020. Anchoring and stabilization of colloidal PdNPs on exfoliated bis-thiourea modified graphene oxide layers with super catalytic activity in water and PEG. *Colloid Surf. A Physicochem. Eng. Asp.* 602. <https://doi.org/10.1016/j.colsurfa.2020.125130> 125130.
- Alsammarraie, F.K., Wang, W., Zhou, P., Mustapha, A., Lin, M., 2018. Green synthesis of silver nanoparticles using turmeric extracts and investigation of their antibacterial activities. *J. Col. Surf. B Bio. Int.* 1, 398–405. <https://doi.org/10.1016/j.colsurfb.2018.07.059>.
- Angulo-Pineda, C., Palma, P.I., Bejarano, J., Riveros, A., Kogan, M. J., Palza, H., 2019. Antibacterial silver nanoparticles supported on graphene oxide with reduced cytotoxicity. *JOM* 71, 10. <https://doi.org/10.1007/s11837-019-03633-2>.
- Ardila, N., Daigle, F., Heuzey, M.-C., Aji, A., 2017. Antibacterial activity of neat chitosan powder and flakes. *Molecules* 22, 100. <https://doi.org/10.3390/molecules22010100>.
- Ashkarran, A.A., Estakhri, S., Nezhad, M.R.H., Eshghi, S., 2013. Controlling the geometry of silver nanostructures for biological applications. *Phys. Procedia* 40, 76–83. <https://doi.org/10.1016/j.phpro.2012.12.011>.
- Awais, Ali, N., Khan, A., Asiri, A.M., Kamal, T., 2021. Potential application of in-situ synthesized cobalt nanoparticles on chitosan-coated cotton cloth substrate as catalyst for the reduction of pollutants. *Environ. Technol. Innov.* 23, 101675. <https://doi.org/10.1016/j.eti.2021.101675>.
- Basta, M., Annamaraju, P., 2021. *Bacterial Spores*. StatPearls Publishing.
- Behzad, F., Naghib, S.M., Kouhbanani, M.A.J., Tabatabaei, S.N., Zare, Y., Rhee, K.Y., 2020. An overview of the plant-mediated green synthesis of noble metal nanoparticles for antibacterial applications. *J. Ind. Eng. Chem.* <https://doi.org/10.1016/j.jiec.2020.12.005>.
- Chang, A.K.T., Frias Jr, R.R., Alvarez, L.V., Bigol, U.G., Guzman, J. P.M.D., 2019. Comparative antibacterial activity of commercial chitosan and chitosan extracted from *Auricularia* sp. *Biocatal. Agric. Biotechnol.* 17, 189–195. <https://doi.org/10.1016/j.bcab.2018.11.016>.
- Chen, C.-H., Lin, Y.-C., Mao, C.-F., Liao, W.-T., 2019. Green synthesis, size control, and antibacterial activity of silver nanoparticles on chitosan films. *Res. Chem. Intermed.* 45, 4463–4472.
- Cheng, Y.F., Zhang, J.Y., Wang, Y.B., Li, C.M., Lu, Z.S., Hu, X.F., Xu, L.Q., 2019. Deposition of catechol-functionalized chitosan and silver nanoparticles on biomedical titanium surfaces for antibacterial application. *Mater. Sci. Eng. C* 98, 649–656. <https://doi.org/10.1016/j.msec.2019.01.019>.
- Chien, R.-C., Yen, M.-T., Mau, J.-L., 2016. Antimicrobial and antitumor activities of chitosan from shiitake stipes, compared to commercial chitosan from crab shells. *Carbohydr. Polym.* 138, 259–264. <https://doi.org/10.1016/j.carbpol.2015.11.061>.
- Dara, P.K., Mahadevan, R., Digita, P.A., Visuviniyagam, S., Kumar, L.R.G., Mathew, S., Ravishnakar, C.N., Anandan, R., 2020. Synthesis and biochemical characterization of silver nanoparticles grafted chitosan (Chi-Ag-NPs): in vitro studies on antioxidant and antibacterial applications. *SN Appl. Sci.* 2, 665. <https://doi.org/10.1007/s42452-020-2261-y>.

- De Leersnyder, I., Rijckaert, H., De Gelder, L., Van Driessche, I., 2020. High variability in silver particle characteristics, silver concentrations, and production batches of commercially available products indicates the need for a more rigorous approach. *Nanomaterials* 10, 1394. <https://doi.org/10.3390/nano10071394>.
- Divakar, D.D., Jastaniyah, N.T., Altamimi, H.G., Alnakhli, Y.O., Muzahed, , Alkheraif, A.A., Haleem, S., 2017. Enhanced antimicrobial activity of naturally derived bioactive molecule chitosan conjugated silver nanoparticle against dental implant pathogens. *Int. J. Biol. Macromol.* 108, 790–797. <https://doi.org/10.1016/j.ijbiomac.2017.10.166>.
- Duran, N., Duran, M., de Jesus, M.B., Seabra, A.B., Favaro, W.J., Nakazato, G., 2016. Silver nanoparticles: A new view on mechanistic aspects on antimicrobial activity. *Nanomedicine* 12, 789–799. <https://doi.org/10.1016/j.nano.2015.11.016>.
- Dutta, T., Chattopadhyay, A.P., Mandal, M., Ghosh, N.N., Mandal, V., Das, M., 2020. Facile green synthesis of silver bionanocomposite with size dependent antibacterial and synergetic effects: a combined experimental and theoretical studies. *J. Inorg. Organomet. Polym. Mater.* 30, 1839–1851. <https://doi.org/10.1016/j.jeece.2020.104019>.
- El-Zahry, M.R., Mahmoud, A., Refaat, I.H., Mohamed, H.A., Bohlmann, H., Lendil, B., 2015. Antibacterial effect of various shapes of silver nanoparticles monitored by SERS. *Talanta* 138, 183–189. <https://doi.org/10.1016/j.talanta.2015.02.022>.
- Errington, J., 2003. Regulation of endospore formation in *Bacillus subtilis*. *Nat. Rev. Microbiol.* 1, 117–126. <https://doi.org/10.1038/nrmicro750>.
- Eymard-Vernain, E., Coute, Y., Adrait, A., Rabilloud, T., Sarret, G., Lelong, C., 2018. The polygamma-glutamate of *Bacillus subtilis* interacts specifically with silver nanoparticles. *PLoS One* 13, 1–19. <https://doi.org/10.1371/journal.pone.0197501>.
- Fan, M., Si, J., Xu, X., Chen, L., Chen, L., Chen, J., Yang, C., Zhu, J., Wu, L., Tian, J., Chen, X., Mou, X., Cai, X., 2021. A versatile chitosan nanogel capable of generating AgNPs in-situ and long-acting slow-release of Ag⁺ for highly efficient antibacterial. *Carbohydr. Polym.* 257, <https://doi.org/10.1016/j.carbpol.2021.117636> 117636.
- Franklin, M.L., Clark, W.A., 1981. Simple, inexpensive, and rapid way to produce *Bacillus subtilis* spores for the Guthrie bioassay. *J. Clin. Microbiol.* 14, 113–115. <https://doi.org/10.1128/JCM.14.1.113-115.1981>.
- Gakiya-Teruya, M., Palomino-Marcelo, L., Rodriguez-Reyes, J., 2019. Synthesis of highly concentrated suspensions of silver nanoparticles by two versions of the chemical reduction method. *Methods Protoc.* 2 (3). <https://doi.org/10.3390/mps2010003>.
- Gambino, M., Marzano, V., Villa, F., Vitali, A., Vannini, C., Landini, P., Cappitelli, F., 2015. Effects of sublethal doses of silver nanoparticles on *Bacillus subtilis* planktonic and sessile cells. *J. Appl. Microbiol.* <https://doi.org/10.1111/jam.12779>.
- García-Serradilla, M., Risco, C., 2021. Light and electron microscopy imaging unveils new aspects of the antiviral capacity of silver nanoparticles in bunyavirus-infected cells. *Virus Res.* 302, <https://doi.org/10.1016/j.virusres.2021.198444> 198444.
- Gerhardt, P., 1981. *Manual of methods for general bacteriology*. American Society for Microbiolog, Washington D.C..
- Ghaseminezhad, S.M., Hamed, S., Shojasoadati, S.A., 2012. Green synthesis of silver nanoparticles by a novel method: Comparative study of their properties. *Carbohydr. Polym.* 89, 467–472. <https://doi.org/10.1016/j.carbpol.2012.03.030>.
- Gonca, S., Arslan, H., Isik, Z., Özdemir, S., Dizge, N., 2021. The surface modification of ultrafiltration membrane with silver nanoparticles using *Verbascum thapsus* leaf extract using green synthesis phenomena. *Surf. Interfaces* 26, <https://doi.org/10.1016/j.surfin.2021.101291> 101291.
- Hada, H., Yonezawa, Y., Yoshida, A., Kurakake, A., 1976. Photoreduction of silver ion in aqueous and alcoholic solution. *J. Phys. Chem.* 80 (25), 2728–2731. <https://doi.org/10.1021/j100566a003>.
- Hamouda, T., Ibrahim, H.M., Kafafy, H.H., Mashaly, H.M., Mohamed, N.H., Aly, N.M., 2021. Preparation of cellulose-based wipes treated with antimicrobial and antiviral silver nanoparticles as novel effective high-performance coronavirus fighter. *Int. J. Biol. Macromol.* 181, 990–1002. <https://doi.org/10.1016/j.ijbiomac.2021.04.071>.
- Hang, A.T., Tae, B., Park, J.S., 2010. Non-woven mats of poly(vinyl alcohol)/chitosan blends containing silver nanoparticles: Fabrication and characterization. *Carbohydr. Polym.* 82, 472–479. <https://doi.org/10.1016/j.carbpol.2010.05.016>.
- Harada, M., Katagiri, E., 2010. Mechanism of silver particle formation during photoreduction using in situ time-resolved SAXS analysis. *Langmuir* 26 (23), 17896–17905. <https://doi.org/10.1021/la102705h>.
- Hashemi, Z., Mizwari, Z.M., Mohammadi-Aghdam, S., Mortazavi-Derazkola, S., Ebrahimzadeh, M.A., 2021. Sustainable green synthesis of silver nanoparticles using *Sambucus ebulus* phenolic extract (AgNPs@SEE): Optimization and assessment of photocatalytic degradation of methyl orange and their in vitro antibacterial and anticancer activity. *Arab. J. Chem.* 103525. <https://doi.org/10.1016/j.arabjc.2021.103525>.
- Hidayat, M.I., Adlim, M., Maulana, I., Zulfajri, M., 2021. Immobilization of Silver Nanoparticles on Chitosan-Coated Silica-Gel-Beads and the Antibacterial Activity. *Key Eng. Mater.* 892, 36–42. <https://doi.org/10.4028/www.scientific.net/kem.892.36>.
- Huang, H., Yuan, Q., Yang, X., 2004. Preparation and characterization of metal-chitosan nanocomposites. *Colloids. Surf. B.* 39, 31–37. <https://doi.org/10.1016/j.colsurfb.2004.08.014>.
- Ifuku, S., Tsukiyama, Y., Yukawa, T., Egusa, M., Kaminaka, H., Izawa, H., Morimoto, M., Saimoto, H., 2015. Facile preparation of silver nanoparticles immobilized on chitin nanofiber surfaces to endow antifungal activities. *Carbohydr. Polym.* 117, 813–817. <https://doi.org/10.1016/j.carbpol.2014.10.042>.
- Ji, S.-M., Tiwari, A.P., Oh, H.J., Kim, H.-Y., 2021. ZnO/Ag nanoparticles incorporated multifunctional parallel side by side nanofibers for air filtration with enhanced removing organic contaminants and antibacterial properties. *Colloids Surf. A Physicochem. Eng. Asp.* 621, <https://doi.org/10.1016/j.colsurfa.2021.126564> 126564.
- Ju, Y., Han, T., Yin, J., Li, Q., Chen, Z., Wei, Z., Zhang, Y., Dong, L., 2021. Bumpy structured nanofibrous membrane as a highly efficient air filter with antibacterial and antiviral property. *Sci. Total Environ.* 777, <https://doi.org/10.1016/j.scitotenv.2021.145768> 145768.
- Kang, H., Buchman, J.T., Rodriguez, R.S., Ring, H.L., He, J., Bantz, K.C., Haynes, C.L., 2019. Stabilization of silver and gold nanoparticles: preservation and improvement of plasmonic functionalities. *Chem. Rev.* 119, 664–699. <https://doi.org/10.1021/acs.chemrev.8b00341>.
- Kanniah, P., Chelliah, P., Thangapandi, J.R., Gnanadhas, G., Mahendran, V., Robert, M., 2021. Green synthesis of antibacterial and cytotoxic silver nanoparticles by *Piper nigrum* seed extract and development of antibacterial silver based chitosan nanocomposite. *Intl. J. Biomol. Macromol.* 189, 18–33. <https://doi.org/10.1016/j.ijbiomac.2021.08.056>.
- Karunamuni, R., Naha, P.C., Lau, K.C., Al-Zaki, A., Popov, A.V., Delikatny, E.J., Tsourkas, A., Cormode, D.P., Maidment, A.D., 2016. Development of silica-encapsulated silver nanoparticles as contrast agents intended for dual-energy mammography. *Eur. Radiol.* 26, 3301–3309. <https://doi.org/10.1007/s00330-015-4152-y>.
- Khorrami, S., Kamali, F., Zarrabi, A., 2020. Bacteriostatic activity of aquatic extract of black peel pomegranate and silver nanoparticles biosynthesized by using the extract. *Biocatal. Agric. Biotechnol.* 25, <https://doi.org/10.1016/j.cbac.2020.101620> 101620.
- Korshed, P., Li, L., Ngo, D.T., Wang, T., 2018. Effect of storage conditions on the long-term stability of bactericidal effects for laser generated silver nanoparticles. *Nanomaterials* 8, 218. <https://doi.org/10.3390/nano8040218>.

- Kumar-Krishnan, S., Prokhorov, E., Hernández-Iturriaga, M., Mota-Morales, J.D., Vázquez-Lepe, M., Kovalenko, Y., Sanches, I.C., Luna-Bárceñas, G., 2015. Chitosan/silver nanocomposites: synergistic antibacterial action of silver nanoparticles and silver ions. *Eur. Polym. J.* 67, 242–251. <https://doi.org/10.1016/j.eurpolymj.2015.03.066>.
- Li, J., Rong, K., Zhao, H., Li, F., Lu, Z., Chen, R., 2013. Highly selective antibacterial activities of silver nanoparticles against *Bacillus subtilis*. *J. Nanosci. Nanotechnol.* 13, 6806–6813. <https://doi.org/10.1166/jnn.2013.7781>.
- Mathur, P., Jha, S., Ramtane, S., Jain, N.K., 2018. Pharmaceutical aspects of silver nanoparticles. *Artif. Cells Nanomed. Biotechnol.* 46, 115–126. <https://doi.org/10.1080/21691401.2017.1414825>.
- Matsumoto, A., Ishikawa, T., Odani, T., Oikawa, H., Okada, S., Nakanishi, H., 2006. An organic/inorganic nanocomposite consisting of poly(muconate and silver nanoparticles. *Macromol. Chem. Phys.* 207, 361–369.
- Mokhena, T.C., Luyt, A.S., 2017. Electrospun alginate nanofibres impregnated with silver nanoparticles: Preparation, morphology and antibacterial properties. *Carbohydr. Polym.* 165, 304–312. <https://doi.org/10.1016/j.carbpol.2017.02.068>.
- Nate, Z., Moloto, M.J., Mubiayi, P.K., Sibiya, P.N., 2018. Green synthesis of chitosan capped silver nanoparticles and their antimicrobial activity. *MRS Adv.* 3, 2505–2517. <https://doi.org/10.1557/adv.2018.368>.
- Nie, W., Dai, X., Li, D., McCoul, D., Gillispie, G.J., Zhang, Y., Yu, B., He, C., 2018. One-pot synthesis of silver nanoparticle incorporated mesoporous silica granules for hemorrhage control and antibacterial treatment. *ACS Biomater. Sci. Eng.* 4, 3588–3599. <https://doi.org/10.1021/acsbmaterials.8b00527>.
- Paramelle, D., Sadovoy, A., Gorelik, S., Free, P., Hobbey, J., Fernig, D.G., 2014. A rapid method to estimate the concentration of citrate capped silver nanoparticles from UV-visible light spectra. *Analyst* 139, 4855–4861. <https://doi.org/10.1039/C4AN00978A>.
- Pardo-Castaño, C., Bolaños, G., 2019. Solubility of chitosan in aqueous acetic acid and pressurized carbon dioxide-water: Experimental equilibrium and solubilization kinetics. *J. Supercrit. Fluids* 151, 63–74. <https://doi.org/10.1016/j.supflu.2019.05.007>.
- Rafńska, K., Pomastowski, P., Buszewski, B., 2019. Study of *Bacillus subtilis* response to different forms of silver. *Sci. Total Environ.* 661, 120–129. <https://doi.org/10.1016/j.scitotenv.2018.12.139>.
- Raman, G., Park, S.J., Sakthivel, N., Suresh, A.K., 2017. Physico-cultural parameters during AgNPs biotransformation with bactericidal activity against human pathogens. *Enzym. Microb. Technol.* 100, 45–51. <https://doi.org/10.1016/j.enzmictec.2017.02.002>.
- Ranjani, B., Pandian, K., Arun Kumar, G., Gonpinath, S.C.B., 2019. D-glucosamine chitosan base molecule-assisted synthesis of different shape and sized silver nanoparticles by a single pot method: A greener approach for sensor and microbial applications. *Int. J. Biol. Macromol.* 133, 1280–1287. <https://doi.org/10.1016/j.ijbiomac.2019.04.196>.
- Raza, M.A., Kanwal, Z., Rauf, A., Sabri, A.N., Riaz, S., Naseem, S., 2016. Size- and shape-dependent antibacterial studies of silver nanoparticles synthesized by wet chemical routes. *Nanomaterials* 6, 74. <https://doi.org/10.3390/nano6040074>.
- Reicha, F.M., Sarhan, A., Abdel-Hamid, M.I., El-Sherbiny, I.M., 2012. Preparation of silver nanoparticles in the presence of chitosan by electrochemical method. *Carbohydr. Polym.* 89, 236–244. <https://doi.org/10.1016/j.carbpol.2012.03.002>.
- Roy, A., Bulut, O., Some, S., Mandal, A.K., Yilmaz, A.M., 2019. Green synthesis of silver nanoparticles: biomolecule-nanoparticle organizations targeting antimicrobial activity. *RSC Adv.* 9, 2673. <https://doi.org/10.1039/C8RA08982E>.
- Senthilkumar, P., Yaswant, G., Kavitha, S., Chandramohan, E., Kowsalya, G., Vijay, R., Sudhagar, B., Ranjith Santosh Kumar, D. S., 2019. Preparation and characterization of hybrid chitosan-silver nanoparticles (Chi-Ag NPs): A potential antibacterial agent. *Int. J. Biol. Macromol.* 141, 290–297. <https://doi.org/10.1016/j.ijbiomac.2019.08.234>.
- Senthilkumar, R.P., Bhuvaneshwari, V., Ranjithkumar, R., Sathiyavimal, S., Malayaman, V., Chandarshekar, B., 2017. Synthesis, characterization and antibacterial activity of hybrid chitosan-cerium oxide nanoparticles: as a bionanomaterials. *Int. J. Biol. Macromol.* 104, 1746–1752. <https://doi.org/10.1016/j.ijbiomac.2017.03.139>.
- Shanmuganathan, R., Karuppusamy, I., Muthupandian, S., Harshiny, M., Ponnuchamy, K., Vijayan, S.R., 2019. Synthesis of silver nanoparticles and their biomedical applications – a comprehensive review. *Curr. Pharm. Des.* 25, 2650–2660. <https://doi.org/10.2174/1381612825666190708185506>.
- Siripatrawan, U., Vitthayakitti, W., 2016. Improving functional properties of chitosan films as active food packaging by incorporating with propolis. *Food Hydrocoll.* 61, 695–702. <https://doi.org/10.1016/j.foodhyd.2016.06.001>.
- Sukhov, N.L., Ershov, N.B., Mikhalko, K., Gordeev, A.V., 1997. Absorption spectra of large colloidal silver particles in aqueous solution. *Russ. Chem. Bull.* 46 (1), 197–199. <https://doi.org/10.1007/BF02495374>.
- Sundaram, J., Pant, J., Goudie, M.J., Mani, S., Handa, H., 2016. Antimicrobial and physicochemical characterization of biodegradable, nitric oxide-releasing nanocellulose–chitosan packaging membranes. *J. Agric. Food Chem.* 64, 5260–5266. <https://doi.org/10.1021/acs.jafc.6b01936>.
- Targhi, A., Moammeri, A., Jamshidifar, E., Abbaspour, K., Sadeghi, S., Lamakani, L., Akbarzadeh, I., 2021. Synergistic effect of curcumin-Cu and curcumin-Ag nanoparticle loaded niosome: Enhanced antibacterial and anti-biofilm activities. *Bioorg. Chem.* 115. <https://doi.org/10.1016/j.bioorg.2021.105116> 105116.
- Twu, Y.-K., Chen, Y.-W., Shih, C.-M., 2008. Preparation of silver nanoparticles using chitosan suspensions. *Powder Technol.* 185, 251–257. <https://doi.org/10.1016/j.powtec.2007.10.025>.
- Valencia, A.M., Valencia, C.H., Zuluaga, F., Grande-Tovar, C.D., 2021. Synthesis and fabrication of films including graphene oxide functionalized with chitosan for regenerative medicine applications. *Heliyon* 7, (5). <https://doi.org/10.1016/j.heliyon.2021.e07058> e07058.
- Velusamy, P., Chia-Hung, S., Shritama, A., Kumar, G.V., Jeyanthi, V., Pandian, K., 2016. Synthesis of oleic acid coated iron oxide nanoparticles and its role in anti-biofilm activity against clinical isolates of bacterial pathogens. *Rev. Mex. Urol.* 76, 450–456. <https://doi.org/10.1016/j.jtice.2015.07.018>.
- Venkatesan, J., Lee, J.-Y., Kang, D.S., Anil, S., Kim, S.-K., Shim, M. S., Kim, D.G., 2017. Antimicrobial and anticancer activities of porous chitosan-alginate- biosynthesized silver nanoparticles. *Int. J. Biol. Macromol.* 97, 515–525. <https://doi.org/10.1016/j.ijbiomac.2017.01.120>.
- Wang, L., Hu, C., Shao, L., 2017. The antimicrobial activity of nanoparticles: Present situation and prospects for the future. *Int. J. Nanomed.* 12, 1227–1249. <https://doi.org/10.2147/IJN.S121956>.
- Wang, L.S., Wang, C.Y., Yang, C.H., Hsieh, C.L., Chen, S.Y., Shen, C.Y., Wang, J.J., Huang, K.S., 2015. Synthesis and anti-fungal effect of silver nanoparticles–chitosan composite particles. *Int. J. Nanomed.* 65, 2685–2696. <https://doi.org/10.2147/IJN.S77410>.
- Wang, M., Bi, S., Qin, D., Su, C., Wang, H., Chen, X., 2021. Quantitative evaluation of the antibacterial effectiveness and efficiency of chitosan considering the effect of neutralization. *Carbohydr. Polym.* 265. [https://doi.org/10.1016/j-carbpol.2021.117918](https://doi.org/10.1016/j.carbpol.2021.117918) 117918.
- Wijesena, R.N., Tissera, N.D., Rathnayaka, V.W.S.G., de Silva, R.M., de Silva, K.M.N., 2020. Colloidal stability of chitin nanofibers in aqueous systems: effect of pH, ionic strength, temperature & concentration. *Carbohydr. Polym.* 235. <https://doi.org/10.1016/j.carbpol.2020.116024> 116024.
- Wu, Z., Huang, X., Li, Y.-C., Xiao, H., Wang, X., 2018. Novel chitosan films with laponite immobilized Ag nanoparticles for active food packaging. *Carbohydr. Polym.* 199, 210–218. <https://doi.org/10.1016/j.carbpol.2018.07.030>.

- Xu, Q., Zheng, W., Duan, P., Chen, J., Zhang, Y., Fu, F., Diao, H., Liu, X., 2019. One-pot fabrication of durable antibacterial cotton fabric coated with silver nanoparticles via carboxymethyl chitosan as a binder and stabilizer. *Carbohydr. Polym.* 204, 42–49. <https://doi.org/10.1016/j.carbpol.2018.09.089>.
- Ye, H., Cheng, J., Yu, K., 2019. In situ reduction of silver nanoparticles by gelatin to obtain porous silver nanoparticle/chitosan composites with enhanced antimicrobial and wound-healing activity. *Int. J. Biol. Macromol.* 121, 633–642. <https://doi.org/10.1016/j.ijbiomac.2018.10.056>.
- Zhang, W., Mou, Z., Wang, Y., Chen, Y., Yang, E., Guo, F., Sun, D., Wang, W., 2019. Molybdenum disulfide nanosheets loaded with chitosan and silver nanoparticles effective antifungal activities: in vitro and in vivo. *Mater. Sci. Eng. C* 97, 486–497. <https://doi.org/10.1016/j.msec.2018.12.052>.
- Zhang, W., Xiao, B., Fang, T., 2018. Chemical transformation of silver nanoparticles in aquatic environments: mechanism, morphology and toxicity. *Chemosphere* 191, 324–334. <https://doi.org/10.1016/j.chemosphere.2017.10.016>.
- Zhang, X.-F., Liu, Z.-G., Shen, W., Gurunathan, S., 2016. Silver nanoparticles: synthesis, characterization, properties, applications, and therapeutic approaches. *Int J Mol Sci.* 17, 1534. <https://doi.org/10.3390/ijms17091534>.
- Zielinska, A., Skwarek, E., Zaleska, A., Gazda, M., Hupkam, J., 2009. Preparation of silver nanoparticles with controlled particle size. *Procedia Chem.* 1, 1560–1566. <https://doi.org/10.1016/j.proche.2009.11.004>.
- Zienkiewicz-Strzałka, M., Deryło-Marczewska, A., Skorik, Y.A., Petrova, V.A., Choma, A., Komanięcka, I., 2019. Silver nanoparticles on chitosan/silica nanofibers: characterization and antibacterial activity. *Int. J. Mol. Sci.* 21, 166. <https://doi.org/10.3390/ijms21010166>.
- Zong, R., Wang, X., Shi, S., Zhu, Y., 2014. Kinetically controlled seed-mediated growth of narrow dispersed silver nanoparticles up to 120 nm: secondary nucleation, size focusing, and Ostwald ripening. *Phys. Chem. Chem. Phys.* 16, 4236–4241. <https://doi.org/10.1039/C3CP54846E>.